AIP Applied Physics Letters

Room temperature photoluminescence from InxAl(1−x)N films deposited by plasma-assisted molecular beam epitaxy

W. Kong, A. Mohanta, A. T. Roberts, W. Y. Jiao, J. Fournelle, T. H. Kim, M. Losurdo, H. O. Everitt, and A. S. Brown

Citation: Applied Physics Letters **105**, 132101 (2014); doi: 10.1063/1.4896849
View online: http://dx.doi.org/10.1063/1.4896849
View Table of Contents: http://scitation.aip.org/content/aip/journal/apl/105/13?ver=pdfcov
Published by the AIP Publishing

APPLIED PHYSICS LETTERS **105**, 132101 (2014)

Room temperature photoluminescence from $In_xAl_{(1-x)}N$ films deposited by plasma-assisted molecular beam epitaxy

W. Kong,[1,a)] A. Mohanta,[2] A. T. Roberts,[3] W. Y. Jiao,[1] J. Fournelle,[4] T. H. Kim,[1] M. Losurdo,[5] H. O. Everitt,[3,6] and A. S. Brown[1]

[1]*Department of Electrical and Computer Engineering, Duke University, Durham, North Carolina 27708, USA*
[2]*Oak Ridge Institute for Science and Education, Research Participation Program, U.S. Army Aviation and Missile Research, Development and Engineering Center (AMRDEC), Redstone Arsenal, Alabama 35898, USA*
[3]*Charles Bowden Research Lab, Army Aviation & Missile RD&E Center, Redstone Arsenal, Alabama 35898, USA*
[4]*Department of Geoscience, University of Wisconsin, Madison, Wisconsin 53706, USA*
[5]*Plasma Chemistry Research Center-CNR, via Orabona, 4-70126 Bari, Italy*
[6]*Department of Physics, Duke University, Durham, North Carolina 27708, USA*

(Received 30 July 2014; accepted 18 September 2014; published online 29 September 2014)

InAlN films deposited by plasma-assisted molecular beam epitaxy exhibited a lateral composition modulation characterized by 10–12 nm diameter, honeycomb-shaped, columnar domains with Al-rich cores and In-rich boundaries. To ascertain the effect of this microstructure on its optical properties, room temperature absorption and photoluminescence characteristics of $In_xAl_{(1-x)}N$ were comparatively investigated for indium compositions ranging from $x = 0.092$ to 0.235, including $x = 0.166$ lattice matched to GaN. The Stokes shift of the emission was significantly greater than reported for films grown by metalorganic chemical vapor deposition, possibly due to the phase separation in these nanocolumnar domains. The room temperature photoluminescence also provided evidence of carrier transfer from the InAlN film to the GaN template. © *2014 AIP Publishing LLC*. [http://dx.doi.org/10.1063/1.4896849]

$In_xAl_{(1-x)}N$ is of great interest for a range of electronic and optoelectronic applications, especially deep ultraviolet (DUV) light emitters and high electron mobility transistors (HEMTs) because its bandgap can be tuned from 0.7–6.2 eV, if grown across the alloy range.[1–3] GaN/InAlN heterojunctions possess large polarization charge densities, and alloys of $In_xAl_{(1-x)}N$ with indium composition $x \approx 0.166$ are of particular interest for III-Nitride heterojunction devices because they are lattice-matched to GaN.[4] However, the synthesis of InAlN is challenging due to the large binding energy difference between InN and AlN, causing an alloy miscibility gap.[5] Reported properties of InAlN vary significantly depending on the specific growth method and conditions. The reason for this is not well understood but likely reflects differences in the structural properties of the films, such as differences in microstructure, compositional uniformity, and strain.

The majority of InAlN films are grown by metalorganic chemical vapor deposition (MOCVD).[6–8] The optical gap of $In_xAl_{(1-x)}N$ is traditionally described by the Vegard's law as $E_A = xE_{InN} + (1-x)E_{AlN} - bx(1-x)$, a curve with downward bowing between the bandgap energies for InN (E_{InN}) and AlN (E_{AlN}). The amplitude of the bowing parameter b of InAlN is reported in the literature varies from 3 to 6 eV, which is greater than the 1.4 eV range in b values found for InGaN alloys.[6–9] Films are also found to exhibit a relatively large Stokes shift varying from 0.5 eV up to ~1–2 eV.[6,7,10,11]

The optical properties of Al-rich ($x < 0.5$) $In_xAl_{(1-x)}N$ films grown by plasma-assisted molecular beam epitaxy (PAMBE) have been much less studied,[12–14] in part, because growth of such films is more challenging than by MOCVD. While the ideal growth temperature for synthesizing AlN is over 800 °C, the typical growth temperature for synthesizing InAlN by PAMBE is usually in the 400 °C–560 °C range due to the temperature-dependent trade-off between enhancing Al migration and inhibiting InN decomposition and In desorption. In addition, PAMBE-grown InAlN exhibits a characteristic honeycomb-shaped nanocolumnar microstructure composed of Al-rich cores and In-rich boundaries with domain diameters of 10–12 nm.[15–17] The absolute In composition in the boundaries is estimated to be as much as 30% higher than in the cores.[16,17] Due to the size of the nanocolumnar microstructure, identification and characterization of the features is difficult, and transmission electron microscopy (TEM) is typically used to characterize the microstructure. To date, only absorption-based measurements have been reported,[12–14] and the modification of InAlN optical characteristics resulting from the nanocolumnar microstructure has not been studied.

Here, we report the fabrication of numerous $In_xAl_{(1-x)}N$ thin films by PAMBE with In composition spanning $x = 0.092$ to 0.235, including $x = 0.166$ lattice matched to GaN. Room temperature photoluminescence (PL) is observed from PAMBE-grown Al-rich InAlN. Structural and optical characterization of these films is performed and comparatively analyzed. TEM analysis reveals PAMBE-synthesized InAlN produces oriented nanocolumnar microstructures, and all but the $In_{0.235}Al_{0.765}N$ films are fully strained to the GaN template. The narrowest x-ray diffraction line widths are found near the $x \approx 0.166$ lattice matching condition and are superior to values reported in the literature.[7,18] In comparison with MOCVD-grown InAlN films, it is found that the Stokes shift of the emission from the absorption edge

a)Author to whom correspondence should be addressed. Electronic mail: wei.kong@duke.edu

is significantly greater, possibly due to the nanocolumnar phase separation observed in PAMBE-grown InAlN. The data also provide evidence of carrier transfer from the InAlN film to the GaN template.

A Veeco Gen II radio frequency PAMBE system deposited InAlN thin films on 10 μm thick hydride vapor phase epitaxy (HVPE) GaN templates. On top of the GaN templates, 50–100 nm thick GaN buffer layers were deposited at 680° using Ga-rich conditions, then InAlN films were deposited at pyrometer-measured temperatures from 400 °C to 540 °C. The N_2 plasma condition was set to 350 W and 1.0 sccm. A Panalytical X'Pert PRO MRD high-resolution x-ray diffraction system (HRXRD) equipped with a 4-bounce Ge (220) hybrid monochromator and triple-axis diffractometry was used to ascertain the composition and structural characteristics of the InAlN samples. The composition of samples was further confirmed by wavelength dispersive (WDS) electron probe micro-analysis (EPMA) with a CAMECA SX51. Surface characterization was performed with a Digital Instruments Dimension 3100 atomic force microscope (AFM), and the absorption characteristics of samples were measured *in situ* with a Horiba-HJ UVISEL spectroscopic ellipsometer (SE). The PL experiment was performed at room temperature using pulsed excitation at 248 nm from an optical parametric amplifier driven by an amplified 800 nm mode-locked fiber laser with 1 kHz repetition rate and 130 fs pulse width. The PL spectra were recorded using a Princeton Instruments Spec-10 liquid nitrogen-cooled charge-coupled device (CCD) attached to a 30 cm grating spectrometer.

Fig. 1(a) shows representative (0002) $\omega/2\theta$ HRXRD scans for a range of $In_xAl_{(1-x)}N$ from $x = 0.114$ to 0.235. The InAlN diffraction peak is to the right of the bright GaN peak, and the associated Pendellosung fringes indicate that the samples possess abrupt interfaces and smooth surfaces. The period of the fringes is used to estimate the sample thickness. AFM measurements (not shown) indicate root-mean square (RMS) surface roughness smaller than 0.7 nm. Accurate composition estimates are critical to relating structural characteristics to the optical response of samples. Since the series of samples have different amounts of strain, we estimate sample composition by measuring the InAlN peak shift with respect to the GaN peak in a $(10\bar{1}5)$ reciprocal space map (RSM). The result is confirmed by EPMA for a more accurate composition determination. Compositions estimated using the (0002) $\omega/2\theta$ peak separations are greater than the values obtained by EPMA and RSM by 1%–2%.

Fig. 2(a) shows representative $(10\bar{1}5)$ RSM peaks for five of the InAlN films. All but one of these InAlN films are fully strained to the GaN template, evidenced by the observation that the asymmetrical reciprocal space InAlN peaks are aligned to the GaN peak along the x axis. The exception is the $In_{0.235}Al_{0.765}N$ film, which is found to be 40% relaxed. The relaxation of this sample is not observable in $(10\bar{1}5)$ RSM as a result of the overlapping of InAlN and GaN peaks, but it is obvious in higher angle scan in $(20\bar{2}5)$ plane as shown in Fig. 2(b). Relaxation of III-Nitride epilayers is usually accompanied by the degradation of composition uniformity, leading to band-tail states and carrier localization.[5]

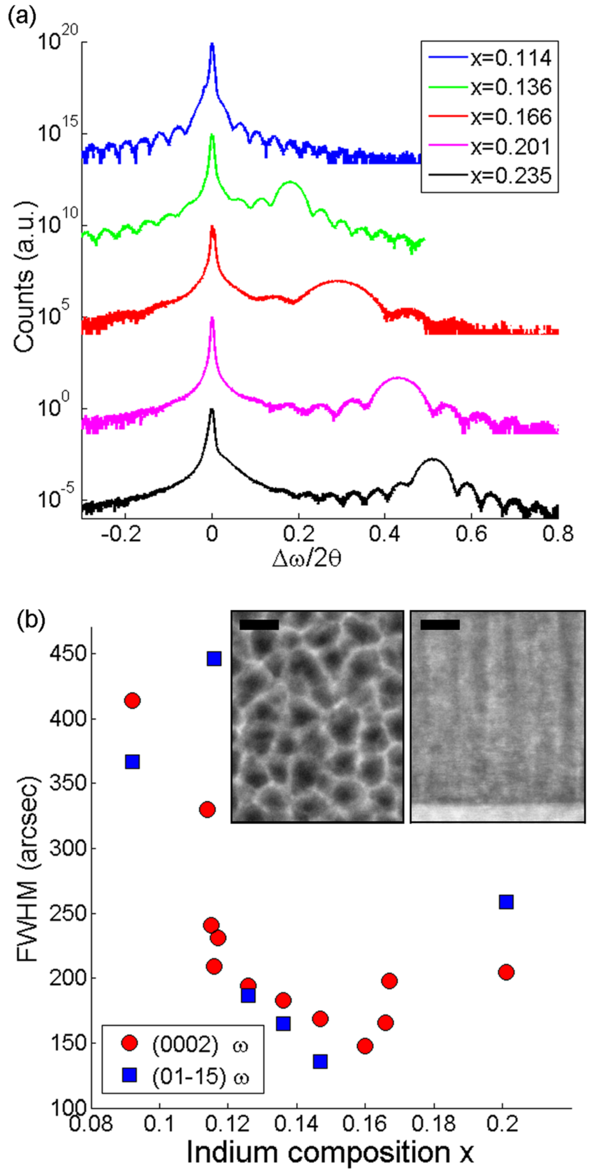

FIG. 1. (a) Representative (0002) $\omega/2\theta$ HRXRD diffraction spectra of several $In_xAl_{(1-x)}N$ films (logarithmic vertical scale). (b) FWHM of the InAlN Bragg peak in two ω directions as a function of x for all $In_xAl_{(1-x)}N$ films. Insets are plan-view (left) and cross-sectional (right) HAADF images of a representative InAlN sample. The black bars at the upper left corners are 12 nm long.

The overall structural quality of the samples is estimated using the HRXRD ω scan in the (0002) and $(10\bar{1}5)$ planes. Peak broadening in the ω direction reflects the lattice periodicity in the associated plane, and dislocations, alloy inhomogeneities, and defects increase that broadening. As Fig. 1(b) indicates, broadening in the ω direction for the (0002) and $(10\bar{1}5)$ planes decreases as the near lattice-match composition ($x = 0.166$) is approached. The observed full width at half maximum (FWHM) values of 148 arc sec in the (0002) plane and 136 arc sec in the $(10\bar{1}5)$ plane are among the best reported in the literature for InAlN.[7,18] However, electron microscopy reveals that these samples possess the nanocolumnar microstructure typical of MBE-grown InAlN. The insets in Fig. 1(b) show plan-view and cross-sectional high angle annular dark field (HAADF) images of a representative InAlN sample. This compositionally modulated

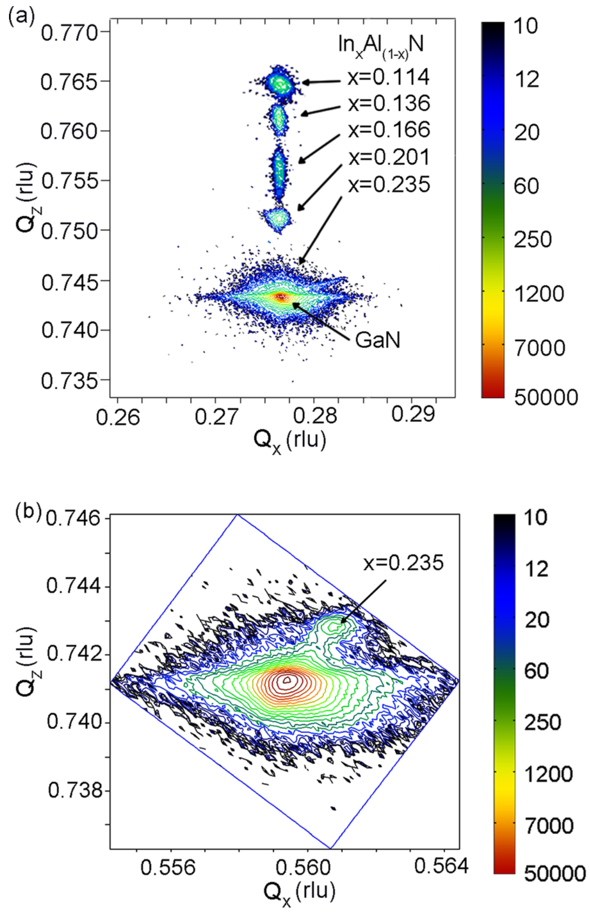

FIG. 2. (a) HRXRD (10$\bar{1}$5) reciprocal space mapping diffraction patterns of $In_xAl_{(1-x)}N$ films with representative composition. (b) HRXRD (20$\bar{2}$5) reciprocal space mapping diffraction patterns of $In_xAl_{(1-x)}N$ films with x = 0.235. The intensity contour is a logarithmic scale divided into 21 levels, and Q_z and Q_x are reciprocal space vectors in reciprocal lattice units (rlu).

microstructure shows the same In-rich boundary regions and Al-rich cores distributed in 10–12 nm columns as that which has been reported extensively by other researchers.[15–17] TEM analysis reveals that the Al-rich cores are of relatively high structural quality, while the In-rich boundaries possess a distorted lattice with varying In composition.[16,17] This microstructure is common to InAlN films synthesized by MBE, with the exception of a recent report on compositionally uniform InAlN grown by MBE under N-rich conditions (III/V ratio = 0.3) at a very slow growth rate (~1 nm/min).[19] These conditions are far from those used in this study and electron microscopy confirms that our films possess this microstructure.

Spectroscopic ellipsometry obtains the dielectric functions of the InAlN layers from the measured ellipsometric parameters Ψ and Δ. After accounting for the SE response of the GaN templates measured at room temperature prior to deposition, the dielectric function of InAlN is obtained using a two-layer Tauc-Lorentz model. The refractive index n and the interband absorption coefficient α are derived from the real and imaginary parts of the dielectric function of sample, $\varepsilon_r(\hbar\omega)$ and $\varepsilon_i(\hbar\omega)$. Because the interband absorption coefficient is related to the band-tail energy as $\alpha(\hbar\omega) \propto (\hbar\omega - E_A)^{1/2}$ using a parabolic bandgap approximation, the band-tail energy may be obtained by linearly extrapolating

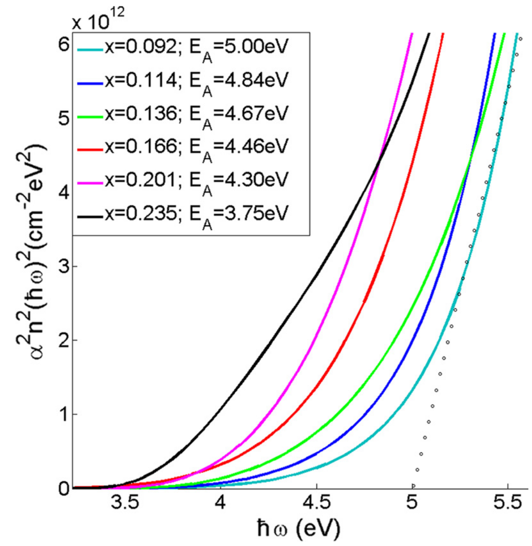

FIG. 3. The absorption edge of representative $In_xAl_{(1-x)}N$ samples obtained by SE, overlaid by an example extrapolation to indicate how E_A is estimated.

the function $\alpha^2 n^2(\hbar\omega)^2$ to zero, where $\hbar\omega$ is the photon energy.[13]

Fig. 3 shows the evolution of the band-tail energy with increasing In composition. In general, the InAlN band-tail red shifts with increasing In composition, and most of the samples have an absorption band-tail with similar slopes. However, the absorption curve of the highest In composition sample ($In_{0.235}Al_{0.765}N$) has a relatively flat band-tail near 3.75 eV, plus a second high energy band-tail of about 5.3 eV (not shown in the figure). InAlN films grown in the mid-composition range are thermodynamically more susceptible to phase separation due to spinodal decomposition,[20] and similar two-step behavior has been observed in $In_xAl_{(1-x)}N$ thin films with $x = 0.4$.[14]

Fig. 4 shows the room temperature photoluminescence spectra for these films. Emission from the GaN templates on which the $In_xAl_{(1-x)}N$ thin films are grown is observed in all

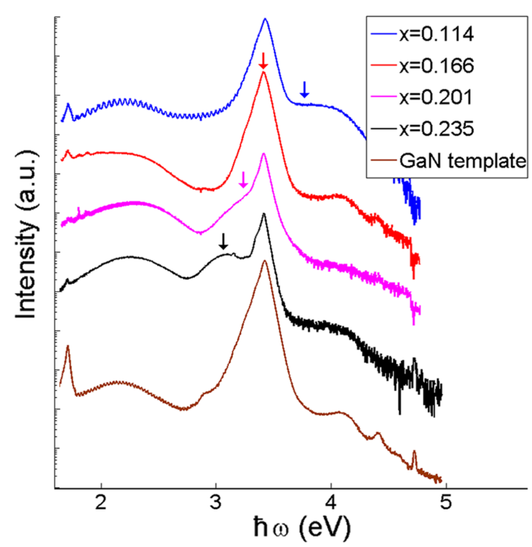

FIG. 4. Room temperature PL spectra of $In_xAl_{(1-x)}N$ thin films. The arrow shows the peak energies of the $In_xAl_{(1-x)}N$ emission bands deduced from Gaussian lineshape fitting. For clarity, the intensity is plotted logarithmically.

spectra. The narrow peak near 3.41 eV is produced by free-exciton recombination near the band-edge, and the broad feature centered near 2.2 eV is the well-known yellow luminescence band in GaN.[21] An additional weak PL peak arises from the $In_xAl_{(1-x)}N$ film and shifts from the higher to the lower energy side of the GaN excitonic emission as x increases. The PL peak energies of $In_xAl_{(1-x)}N$ thin films are estimated using Gaussian curve fitting. For sample, $x = 0.166$, the emission from $In_xAl_{(1-x)}N$ overlaps the GaN near band-tail emission. The room temperature InAlN PL response is not observable for samples with $x = 0.092$ and 0.136, and the PL of the sample with $x = 0.114$ is about two orders of magnitude weaker than that of the GaN template. As x increases, the PL intensity increases as well, and the PL intensity from the $In_{0.235}Al_{0.765}N$ sample is only one order of magnitude smaller than that from the GaN template. Since the majority of the samples possess narrow XRD peaks with FWHM in the ∼150–250 arc sec range, this PL intensity variation does not appear to depend on structural quality.

Fig. 5 shows the variation of the absorption edge (E_A) and the PL peak energy (E_{PL}) of the $In_xAl_{(1-x)}N$ thin films. The x-dependence of E_A and E_{PL} can be linearly fit with slopes of -7.9 ± 0.9 and -6.2 ± 0.4 eV/x, respectively, indicating that both the absorption edges and the PL peak energies redshift with increasing In composition. These redshifts are consistent with a previous report on MOCVD-grown films over this relatively narrow range in x.[7,10] However, the Stokes shift, estimated from the two linear fits, is much larger (0.9 – 1.0 eV) than the best reported values for MOCVD-deposited InAlN (0.5 – 0.7 eV)[7,10] or for AlGaN and InGaN alloys (usually < 0.5 eV).[9,22–25] The larger Stokes shift observed in this study suggests that the PL may arise from carriers localized in the In-rich domains of the nanocolumnar microstructure.

The strength of the GaN PL is also noteworthy considering the SE-measured absorption coefficient of our InAlN samples is approximately 1.54×10^5 cm^{-1} at 248 nm. Consequently, approximately 80% of the excitation is absorbed by the ∼100 nm-thick InAlN films, and even the lone exception

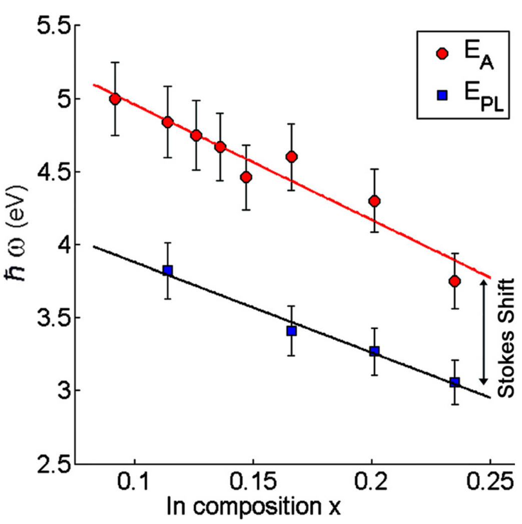

FIG. 5. Measured absorption edges (red) and peak PL emission energies (blue) from the InAlN films, each of which is fit by a linear regression (solid line) from which the Stokes Shift is obtained.

46 nm thick $In_{0.166}Al_{0.834}N$ film absorbs 50%. Since comparatively little pump excitation reaches the GaN template, the strength of the GaN PL from each sample is quite surprising, even considering that the GaN PL energy is well below the absorption band edge (E_A) of the InAlN films. Indeed, compared to the GaN templates, the GaN PL intensity is only reduced 9% in the $In_{0.166}Al_{0.834}N$ sample and only 51% in the $In_{0.114}Al_{0.886}N$ sample. We therefore infer that carriers transferred from the InAlN films with $x = 0.166$ and 0.114 generate 45%–60% of the measured GaN PL, respectively.

Ultrafast carrier transport to a GaN template has been seen in MOCVD-grown InAlN thin films through V-defects that act as carrier transport channels.[26] Because TEM and AFM analysis of our PAMBE $In_{0.114}Al_{0.886}N$ and $In_{0.166}Al_{0.834}N$ samples indicate a very low density of V-defects, we infer that carrier transport is mediated by the nanocolumnar microstructure with numerous edge-type threading dislocations. Consequently, some carriers photo-generated in the InAlN film are transported to the GaN templates to generate strong GaN PL, while others become localized in the In-rich boundaries of the InAlN microstructure to generate InAlN PL with large Stokes shifts.

In conclusion, we systematically examined the structural and optical properties of MBE-grown $In_xAl_{(1-x)}N$ films using high resolution X-ray diffraction, spectroscopic ellipsometry, and PL spectroscopy. Room temperature PL is observed from PAMBE-grown, Al-rich InAlN films. The large (∼1 eV) Stokes shifts observed were likely caused by the composition modulation that produced carrier localization within the nanocolumnar microstructure. The strength of the GaN PL spectra also suggests carrier transfer from the InAlN film to the GaN template.

The authors would like to acknowledge the support of ONR N00014-08-1-0396, GOALI NSF NSF-ECCS-12-02132. This research was supported in part by appointment of A. Mohanta to the Postgraduate Research Participation Program at the U.S. Army Aviation and Missile Research, Development and Engineering Center (AMRDEC) administered by the Oak Ridge Institute for Science and Education through an interagency agreement between the U.S. Department of Energy and AMRDEC.

[1] R. Butté, J. F. Carlin, E. Feltin, M. Gonschorek, S. Nicolay, G. Christmann, D. Simeonov, A. Castiglia, J. Dorsaz, H. J. Buehlmann, S. Christopoulos, G. Baldassarri Höger von Högersthal, A. J. D. Grundy, M. Mosca, C. Pinquier, M. A. Py, F. Demangeot, J. Frandon, P. G. Lagoudakis, J. J. Baumberg, and N. Grandjean, J. Phys. D: Appl. Phys. **40**, 6328 (2007).
[2] A. Yamamoto, Md. R. Islam, T. T. Kang, and A. Hashimoto, Phys. Stat. Sol. C **7**(5), 1309 (2010).
[3] D. S. Lee, X. Gao, S. Guo, D. Kopp, P. Fay, and T. Palacios, IEEE Electron. Device Lett. **32**, 1525 (2011).
[4] M. Gonschorek, J.-F. Carlin, E. Feltin, M. A. Py, and N. Grandjean, Appl. Phys. Lett. **89**, 062106 (2006).
[5] Q. Y. Wei, T. Li, Y. Huang, J. Y. Huang, Z. T. Chen, T. Egawa, and F. A. Ponce, Appl. Phys. Lett. **100**, 092101 (2012).
[6] T. Onuma, S. F. Chichibu, Y. Uhinuma, T. Sota, and S. Yamaguchi, J. Appl. Phys. **94**, 2449 (2003).
[7] J.-F. Carlin, C. Zellweger, J. Dorsaz, S. Nicolay, G. Christmann, E. Feltin, R. Butté, and N. Grandjean, Phys. Stat. Sol. B **242**, 2326 (2005).
[8] E. Sakalauskas, H. Behmenburg, C. Hums, P. Schley, G. Rossbach, C. Giesen, M. Heuken, H. Kalisch, R. H. Jansen, J. Bläsing, A. Dadgar, A. Krost, and R. Goldhahn, J. Phys. D: Appl. Phys. **43**, 365102 (2010).

[9]J. Wu, W. Walukiewicz, K. M. Yu, J. W. Ager III, E. E. Haller, H. Lu, and W. J. Schaff, Appl. Phys. Lett. **80**, 4741 (2002).
[10]K. Wang, R. W. Martin, D. Amabile, P. R. Edwards, S. Hernandez, E. Nogales, K. P. O'Donnell, K. Lorenz, E. Alves, V. Matias, A. Vantomme, D. Wolverson, and I. M. Watson, J. Appl. Phys. **103**, 073510 (2008).
[11]J. F. Carlin and M. Llegems, Appl. Phys. Lett. **83**, 668 (2003).
[12]M. Androulidaki, N. T. Pelekanos, K. Tsagaraki, E. Dimakis, E. Iliopoulos, A. Adikimenakis, E. Bellet-Amealric, D. Jalabert, and A. Georgakilas, Phys. Stat. Sol. C **3**, 1866 (2006).
[13]E. Lliopoulos, A. Adikimenakis, C. Giesen, M. Heuken, and A. Georgakilas, Appl. Phys. Lett. **92**, 191907 (2008).
[14]R. E. Jones, T. Broesler, K. M. Yu, J. W. Ager III, E. E. Haller, W. Walukiewicz, X. Chen, and W. J. Schaff, J. Appl. Phys. **104**, 123501 (2008).
[15]S. Choi, F. Wu, R. Shivaraman, E. C. Young, and J. S. Speck, Appl. Phys. Lett. **100**, 232102 (2012).
[16]L. Zhou, D. J. Smith, and M. R. Mccartney, Appl. Phys. Lett. **90**, 081917 (2007).
[17]S. L. Sahonta, G. P. Dimitrakopulos, T. Kehagias, J. Kioseoglou, A. Adikimenakis, E. Lliopoulos, A. Georgakilas, H. Kirmse, W. Neumann, and P. Komninou, Appl. Phy. Lett. **95**, 021913 (2009).
[18]G. Liu, J. Zhang, X.-H. Li, G. S. Huang, T. Paskova, K. R. Evans, H. Zhao, and N. Tansu, J. Cryst Growth **340**, 66–73 (2012).
[19]S. W. Kaun, El Ahmadi, B. Mazumder, F. Wu, E. C. H. Kyle, P. G. Burke, U. K. Mishra, and J. S. Speck, Semicond. Sci. Technol. **29**, 045011 (2014).
[20]M. Razeghi and M. Henini, *Optoelectronic Devices: III-Nitrides*, (Elsevier, Oxford, 2004), p. 467.
[21]M. A. Reshchikov and H. Morkoc, J. Appl. Phys. **97**, 061301 (2005).
[22]Y. H. Cho, G. H. Gainer, J. B. Lam, J. J. Song, W. Yang, and W. Jhe, Phys. Rev. B **61**, 7203 (2000).
[23]C. Sasaki, H. Naito, M. Iwata, H. Kudo, Y. Yamada, T. Taguchi, T. Jyouichi, H. Okagawa, K. Tadatomo, and H. Tanaka, J. Appl. Phys. **93**, 1642 (2003).
[24]J. P. Zhang, H. M. Wang, M. E. Gaevski, C. Q. Fareed, J. W. Yang, G. Simin, and M. A. Khan, Appl. Phys. Lett. **80**, 3542 (2002).
[25]S. Srinivasan, F. Bertram, A. Bell, and F. A. Ponce, Appl. Phys. Lett. **80**, 550 (2002).
[26]V. Liuolia, S. Marcinkevičius, D. Billingsley, M. Shatalov, J. Yang, R. Gaska, and M. S. Shur, Appl. Phys. Lett. **100**, 242104 (2012).